

Activity of Iron Oxide in Slag with Nepheline Syenite Added as a Flux

Yusaku SAKAMOTO,¹⁾ Keijiro SAITO²⁾ and Masakatsu HASEGAWA^{2)*}

1) Graduate Student, Kyoto University. Now at TAKADA, TAKAHASHI & PARTNERS, 12-22, Tsukiji 1-chome, Chuo-ku, Tokyo, 104-0045 Japan.

2) Department of Energy Science and Technology, Kyoto University, Yoshida-hon-machi, Sakyo-ku, Kyoto, 606-8501 Japan.

(Received November 20, 2023; Accepted February 6, 2024; Advance online published February 15, 2024; Published April 15, 2024)

Although fluorspar has been widely used as a flux for steelmaking slag, there is a strong incentive to explore alternatives. As one of the candidates for such substances, “nepheline syenite” has been investigated in terms of slag fluidity and lime dissolution rate. The present study aimed at clarifying the homogeneous liquid region and Fe_xO activities in the $\text{CaO-Fe}_x\text{O}$ slags with nepheline syenite added at 1 673 K. When the molar ratio of nepheline syenite/ CaO was below 0.658, the substitution of CaO with nepheline syenite raised the Fe_xO activity as well as CaF_2 . The effect of the nepheline syenite addition on slag basicity was discussed by means of the reduction-oxidation reaction of $\text{Fe}^{3+}/\text{Fe}^{2+}$.

KEY WORDS: nepheline syenite; phase diagram; FeO activity; reduction-oxidation reaction.

1. Introduction

A typical harmful impurity in steel, phosphorus, is removed from hot metal by the following oxidation reaction in the steelmaking processes.



$$\begin{aligned} \log K(1) &= \log a_{\text{P}_2\text{O}_5} - 5 \log a_{\text{FeO}} - 2 \log (f_{\text{P}} \cdot [\text{mass}\% \text{P}]_{\text{Fe}}) \\ &= 12\,730 / (T / \text{K}) - 20.0^{1)} \dots\dots (2) \end{aligned}$$

, where $[\text{P}]_{\text{Fe}}$ and $[\text{mass}\% \text{P}]_{\text{Fe}}$ represent phosphorus and its mass% content in molten iron, respectively. a_i denotes the activity of component i in slag and f_{P} is the Henrian activity coefficient of phosphorus in molten iron. According to Le Chatelier’s principle, the thermochemical conditions for effective dephosphorization are low temperature, high a_{FeO} , and high f_{P} . In Fe-C-P liquid alloy, f_{P} can be expressed by

$$\log f_{\text{P}} = e_{\text{P}}^{\text{P}} [\text{mass}\% \text{P}]_{\text{Fe}} + e_{\text{P}}^{\text{C}} [\text{mass}\% \text{C}]_{\text{Fe}} \dots\dots (3)$$

, where e_{P}^i is the first-order interaction coefficient in liquid iron. When iron ore is reduced by carbon, carbon dissolved in pig iron not only decreases the liquidus temperature but also increases the value for f_{P} ($e_{\text{P}}^{\text{C}} = 0.126 > 0^{1)}$, both of which are advantageous to phosphorus removal.

Regarding hydrogen reduction aiming at carbon-neutral refining, it was reported that phosphorus would present as an impurity in hydrogen-reduced iron to the same extent

as the carbon-reduced iron,²⁾ although phosphorus was not easily removed from liquid iron without carbon as already described. The contents of other impurities, silicon and manganese, in hydrogen-reduced iron were estimated to be less than those in carbon-reduced iron,²⁾ and most of sulfur would come from coal as a carbon source. Therefore, it could be mentioned here that dephosphorization would be the most significant issue in the hydrogen-reduced iron refining process. In addition, it would be difficult for CaO as a dephosphorization agent to dissolve in slags with low SiO_2 and MnO contents. In such unfavorable situations, it is necessary to improve slag fluidity while ensuring high FeO activity in the slag for dephosphorization.

In steelmaking processes, some fluxes are used to decrease slag viscosities, lower temperatures at which liquid phase forms, and increase dissolution rates of lime into slags. Although fluorspar, CaF_2 , has been widely used as such a flux, there is a strong need for alternatives to fluorspar, which causes the emission of hazardous fluoride species. Nepheline and/or nepheline syenite is one of the promising candidates for fluoride-free fluxes. As seen in **Fig. 1(a)**, which is the pseudo-binary phase diagram of $\text{NaAlSiO}_4\text{-KAlSiO}_4$,³⁾ “nepheline” corresponds to the solid solution between NaAlSiO_4 and KAlSiO_4 and has the lowest liquidus temperature at a particular composition of $(\text{Na}_{3/4}\text{K}_{1/4})\text{AlSiO}_4$. “Nepheline syenite” is the natural resource containing nepheline together with albite ($\text{NaAlSi}_3\text{O}_8$) and potash feldspar (KAlSi_3O_8).

The usefulness of nepheline and nepheline syenite has

* Corresponding author: E-mail: hasegawa.masakatsu.7r@kyoto-u.ac.jp

been discussed by several studies in terms of slag fluidity and lime dissolution rate.⁴⁻⁸⁾ Amini *et al.*⁶⁾ investigated the static dissolutions of CaO into CaO–SiO₂–Al₂O₃ slags with fluxing agents. Without fluxing agents, the dissolution of lime was prevented by the formation of the Ca₂SiO₄ layer on solid CaO particles, while the Ca₂SiO₄ layer could not be observed with the addition of nepheline syenite as well as CaF₂. They concluded that such fluxes might prevent the formation Ca₂SiO₄ layer with the net effect of an increased lime dissolution rate. Kingston and Caley⁴⁾ measured the viscosities of calcium aluminate slags with the addition of

CaF₂ and/or nepheline syenite. Based on their experimental results, nepheline syenite fluidized slag was found to exhibit a similar rheological behavior to CaF₂ fluidized slag. There was also the possibility that nepheline syenite stabilized fluorspar by forming an alkali low melting point compound, thereby enhancing the capability of fluorspar as a fluidizer.

From a thermodynamic point of view, it is known that CaF₂ increases the activities of iron oxide in slags resulting in promoting the oxidation reactions of impurities in molten iron.⁹⁾ Ozawa *et al.*¹⁰⁾ measured the Fe_xO activities in the CaO–Fe_xO slags with (Na_{3/4}K_{1/4})AlSiO₄ added, which was synthesized as a typical composition of nepheline. The present study was expended to determine the effect of adding natural resource “nepheline syenite” on the Fe_xO activities in the CaO-based slags while clarifying the composition range where the homogeneous liquid phase occurs. In order to directly compare the Fe_xO activity in nepheline syenite-added slag with that in CaF₂-containing slag, the present experiments were conducted at 1 673 K, the same temperature as the literature on the CaO–CaF₂–Fe_xO ternary system.⁹⁾

Hereafter the following abbreviations are used.



NS = nepheline syenite

L = liquid phase

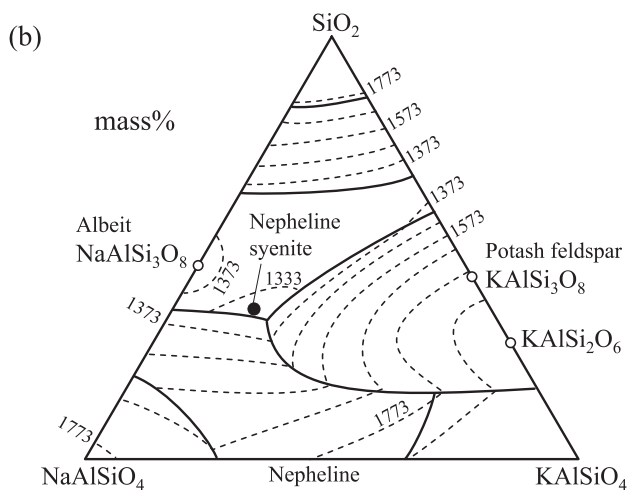
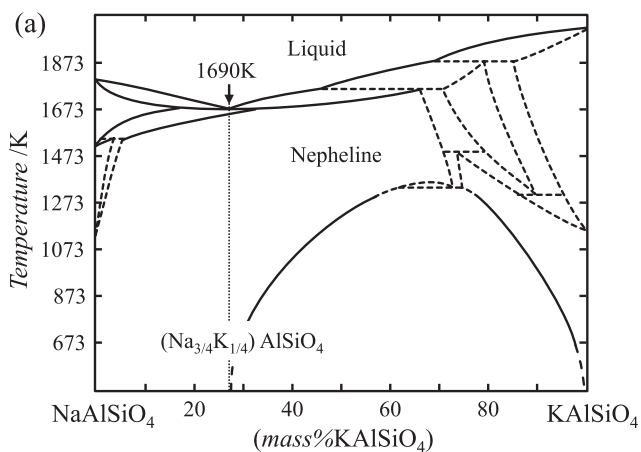


Fig. 1. (a) Phase diagram of NaAlSiO₄–KAlSiO₄ pseudo-binary system.¹⁾ (b) Phase diagram of NaAlSiO₄–KAlSiO₄–SiO₂ pseudo-ternary system.¹⁾

2. Experimental Aspects

Nepheline syenite (NS) used in this study was occurred naturally and from Ontario, Canada. The composition of NS is given in **Table 1** and is plotted on the phase diagram of the NaAlSiO₄–KAlSiO₄–SiO₂ pseudo-ternary system shown in Fig. 1(b).¹⁾ The X-ray diffraction pattern of NS given in **Fig. 2** confirms that NS consists of NaAlSi₃O₈–KAlSi₃O₈ solid solution and KAlSi₂O₆; this is consistent with the phase diagram. As seen in Table 1, NS could be regarded

Table 1. Composition of nepheline syenite.

	SiO ₂	Al ₂ O ₃	Na ₂ O	K ₂ O	others
mass%	60.7	23.3	9.8	4.6	1.6
mole fraction	0.70	0.16	0.11	0.03	–

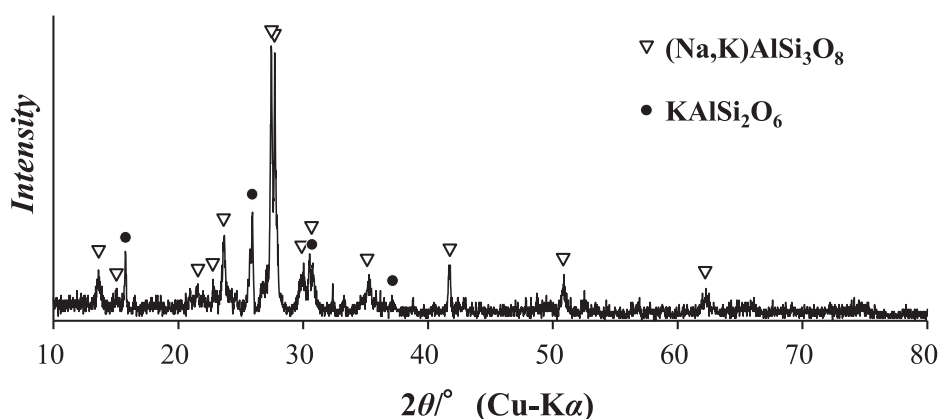


Fig. 2. X-ray diffraction pattern of nepheline syenite occurred naturally.

to be a $\text{Na}_2\text{O}-\text{K}_2\text{O}-\text{Al}_2\text{O}_3-\text{SiO}_2$ quaternary compound since the concentration of the other components is only 1.6 mass%. Table 1 also shows the mole fractions of the quaternary components in NS , and in this study the number of moles of NS , n_{NS} , is defined by Eq. (4).

$$n_{NS} \equiv n_{\text{Na}_2\text{O}} + n_{\text{K}_2\text{O}} + n_{\text{Al}_2\text{O}_3} + n_{\text{SiO}_2} \dots \dots \dots (4)$$

, where n_i is the number of moles of component i .

Reagent-grade Fe , Fe_3O_4 and CaCO_3 were obtained from Nacalai Tesque, Inc., Kyoto, Japan. In order to obtain Fe_xO , Fe and Fe_3O_4 were mixed at a mole ratio of 1:1 and heated at 1 447 K under a stream of argon for 24 hours. X-ray diffraction (XRD) analysis was performed on the resulting compound to confirm the expected oxide phase only. CaO was prepared by decomposing CaCO_3 at 1 273 K. Obtained CaO was mixed with powdery NS at molar ratios n_{CaO}/n_{NS} of 0.117, 0.520, 1.05, 2.79 and 11.5, and pressed into a steel die to form pellets.

The experimental apparatus and procedure have been described in detail elsewhere,¹²⁾ hence only a brief description is given here. **Figure 3** schematically shows the experimental apparatus. An iron crucible of 35 mm o.d., 25 mm i.d., and 100 mm height was charged with pure silver (99.99% pure), and heated under a stream of purified argon inside a SiC resistance furnace. The gas purification train consisted of silica gel, phosphorous pentoxide, and magnesium chips held at 823 K to remove moisture and oxygen remaining in argon. The oxygen probe consisted of a zirconia tube closed at one end as the solid electrolyte and a two-phase mixture of $\text{Mo} + \text{MoO}_2$ as the reference electrode. The zirconia tube

was obtained from Nikkato Corp., Japan and stabilized by 9 mol% of MgO and had 6 mm o.d., 4 mm i.d., and 50 mm length. A molybdenum rod was used as an electrical contact to the reference electrode, while the electrical contact to the outer electrode of the cell was made by the liquid silver and a steel rod soldered to the iron crucible. The oxygen content in liquid silver, which was not determined, would be the equilibrium value corresponding to the oxygen potential between pure solid iron and FeO in slag. Temperature was measured with a Pt-PtRh13 thermocouple and controlled within ± 1 K of the target value by using a PID-type temperature regulator.

When the temperature reached 1 673 K, $\text{CaO} + NS$ pellets and powdery FeO were added to the crucible. About two hours later, an electrochemical oxygen probe was immersed into the liquid silver. The generated cell voltages were monitored on a chart recorder of 1 M Ω internal impedance and simultaneously read by a digital voltmeter of 100 M Ω input resistance with an accuracy of ± 0.01 mV. When the values for electromotive force (*emf*) remained stable, the oxygen probe was replaced with another one to confirm the repeatability of the *emf* measurements. Subsequently, the oxide sample was withdrawn by dipping an iron rod into the slag and cooled rapidly in the air. The collected samples were then submitted to XRD and wet chemical analyses. The detailed procedures of analyses were described below. In order to change the slag compositions, $\text{CaO} + NS$ pellets with the same mixing ratio as the initial one or powdery Fe_xO were added to the slag. During a single experimental run, *emf* reading, sampling, and addition procedures were

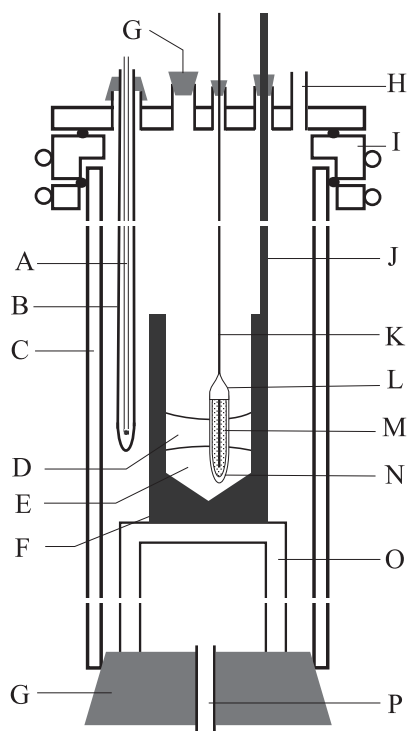


Fig. 3. Experimental apparatus. (A) Pt-PtRh13 thermocouple, (B) Alumina sheath, (C) Mullite reaction tube, (D) Slag, (E) Liquid Ag, (F) Iron crucible, (G) Rubber stopper, (H) Gas outlet, (I) Water-cooled brass flange, (J) Steel rod, (K) Mo rod, (L) Zirconia cement, (M) $\text{Mo} + \text{MoO}_2$ reference electrode, (N) $\text{ZrO}_2(9 \text{ mol}\% \text{MgO})$ solid electrolyte tube, (O) Alumina pedestal, (P) Gas inlet.

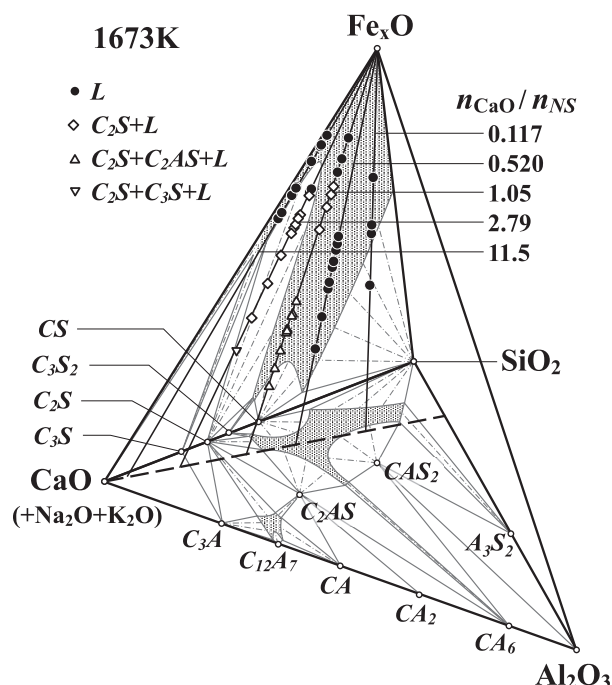


Fig. 4. Experimental compositions with XRD results illustrated in the $(\text{CaO} + \text{Na}_2\text{O} + \text{K}_2\text{O})-\text{Al}_2\text{O}_3-\text{SiO}_2-\text{Fe}_x\text{O}$ pseudo-quaternary tetrahedron. $CS = \text{CaO} \cdot \text{SiO}_2 = \text{CaSiO}_3$, $C_3S_2 = 3\text{CaO} \cdot 2\text{SiO}_2 = \text{Ca}_3\text{Si}_2\text{O}_7$, $C_2S = 2\text{CaO} \cdot \text{SiO}_2 = \text{Ca}_2\text{SiO}_4$, $C_3S = 3\text{CaO} \cdot \text{SiO}_2 = \text{Ca}_3\text{SiO}_5$, $C_3A = 3\text{CaO} \cdot \text{Al}_2\text{O}_3 = \text{Ca}_3\text{Al}_2\text{O}_6$, $C_{12}A_7 = 12\text{CaO} \cdot 7\text{Al}_2\text{O}_3 = \text{Ca}_{12}\text{Al}_4\text{O}_{33}$, $CA = \text{CaO} \cdot \text{Al}_2\text{O}_3 = \text{CaAl}_2\text{O}_4$, $CA_2 = \text{CaO} \cdot 2\text{Al}_2\text{O}_3 = \text{CaAl}_4\text{O}_7$, $CA_6 = \text{CaO} \cdot 6\text{Al}_2\text{O}_3 = \text{CaAl}_{12}\text{O}_{19}$, $A_3S_2 = 3\text{Al}_2\text{O}_3 \cdot 2\text{SiO}_2 = \text{Al}_6\text{Si}_2\text{O}_{10}$, $C_2AS = 2\text{CaO} \cdot \text{Al}_2\text{O}_3 \cdot \text{SiO}_2 = \text{Ca}_2\text{Al}_2\text{SiO}_7$, $CAS_2 = \text{CaO} \cdot \text{Al}_2\text{O}_3 \cdot 2\text{SiO}_2 = \text{CaAl}_2\text{Si}_2\text{O}_8$, $L = \text{liquid phase}$.

repeated at a fixed CaO/NS ratio. **Figure 4** schematically illustrates the (CaO+Na₂O+K₂O)-Al₂O₃-SiO₂-Fe_xO pseudo-quaternary field. The left-side and bottom surfaces of this tetrahedron correspond to the iso-thermal sections of the ternary phase diagrams of CaO-SiO₂-Fe_xO and CaO-SiO₂-Al₂O₃ systems,¹³⁾ respectively. The experimental compositions of slags were changed along the five solid lines passing through the Fe_xO apex shown in Fig. 4.

Concentrations of ferrous iron in slags were determined by dissolving the samples in HCl under a stream of purified argon to avoid oxidation of Fe²⁺ to Fe³⁺, and titrating with standard potassium dichromate.¹⁴⁾ To measure the contents of total iron in slags, the slag samples were dissolved into HCl and submitted to an inductively coupled plasma spectrometer. It can be considered that iron oxide in slags contacting with metallic iron is one component of Fe_xO, and stoichiometric FeO and FeO_{1.5} form Fe_xO.

$$n_{\text{FeO}}\text{FeO} + n_{\text{FeO}_{1.5}}\text{FeO}_{1.5} = n_{\text{Fe}_x\text{O}}\text{Fe}_x\text{O} \dots\dots\dots (5)$$

From stoichiometric relations for iron and oxygen in Eq. (5), the following equations can be obtained, respectively.

$$n_{\text{FeO}} + n_{\text{FeO}_{1.5}} = x \cdot n_{\text{Fe}_x\text{O}} \dots\dots\dots (6)$$

$$n_{\text{FeO}} + 1.5n_{\text{FeO}_{1.5}} = n_{\text{Fe}_x\text{O}} \dots\dots\dots (7)$$

The concentrations of the other components were calculated from the fixed CaO/NS ratios. Considering NS as a Na₂O-K₂O-Al₂O₃-SiO₂ quaternary compound, the mole fraction of Fe_xO, X_{Fe_xO}, in CaO-Na₂O-K₂O-Al₂O₃-SiO₂-Fe_xO slags and x could be expressed by

$$X_{\text{Fe}_x\text{O}} = \frac{n_{\text{Fe}_x\text{O}}}{n_{\text{CaO}} + n_{\text{Na}_2\text{O}} + n_{\text{K}_2\text{O}} + n_{\text{Al}_2\text{O}_3} + n_{\text{SiO}_2} + n_{\text{Fe}_x\text{O}}} \dots (8)$$

$$x = \frac{n_{\text{FeO}} + n_{\text{FeO}_{1.5}}}{n_{\text{FeO}} + 1.5n_{\text{FeO}_{1.5}}} \dots\dots\dots (9)$$

3. Experimental Results and Discussion

3.1. XRD Studies

Figure 5 shows the typical XRD patterns of quenched slag samples. In Fig. 5(a), only a broad peak was observed except for the Fe_xO peaks. Since the experimental temperature 1 673 K was higher than the melting point of Fe_xO, it

could be considered that Fe_xO crystallized during cooling and Sample 2-1 was homogeneous liquid at 1 673 K. On the other hand, Fig. 5(b) confirmed that liquid slag coexisted with the two solid phases of C₂S and C₂AS in the composition of Sample 3-2. The results of the XRD studies are summarized in **Table 2**.

In order to compare the phase relations determined in this study with the reported phase diagrams, Fig. 4 illustrates the experimental compositions with the XRD results in the tetrahedron of (CaO+Na₂O+K₂O)-SiO₂-Al₂O₃-FeO pseudo-quaternary field. The hatched areas on the left-side and bottom correspond to homogeneous liquid regions. The oxides of n_{CaO}/n_{NS} = 0.520 form homogeneous liquids down to relatively low Fe_xO concentrations, while the slags of n_{CaO}/n_{NS} = 1.05 and 2.79 become the two-phase assemblage of C₂S + L in the wide Fe_xO concentration ranges. Such present results are consistent with the phase relations in the CaO-SiO₂-Fe_xO ternary system at 1 673 K¹³⁾ illustrated on the left-side of the tetrahedron. The estimated liquidus curve coexisting with C₂S is drawn by a broken curve on the CaO-NS-Fe_xO pseudo-ternary field, as shown in **Fig. 6**.

3.2. Activity Measurements

The equilibrium oxygen partial pressure between pure solid Fe and Fe_xO in slag, P_{O₂}, can be calculated by the following formula.¹⁵⁾

$$emf = \frac{RT}{F} \ln \frac{P_{\text{O}_2}(\text{ref.})^{1/4} + P_e^{1/4}}{P_{\text{O}_2}^{1/4} + P_e^{1/4}} + E_t \dots\dots\dots (10)$$

, where *emf* is the electromotive force of the cell, *R* is the gas constant, *T* is temperature, *F* is the Faraday constant, *E_t* is the thermo-*emf* between Mo(positive) and Fe(negative), *P_e* is the oxygen partial pressure at which the ionic and the *n*-type electronic conductivities are equal. Values for *E_t* and *P_e* have been reported as

$$\log[P_e / \text{atm}] = 20.40 - 64\,500 / (T / \text{K})^{16)} \dots\dots (11)$$

$$E_t / \text{mV} = -14.69 + 0.0227(T / \text{K})^{17)} \dots\dots\dots (12)$$

The oxygen partial pressure at the reference electrode, P_{O₂}(*ref.*), is given by

$$\log[P_{\text{O}_2}(\text{ref.}) / \text{atm}] = 8.84 - 30\,100 / (T / \text{K})^{18)} \dots (13)$$

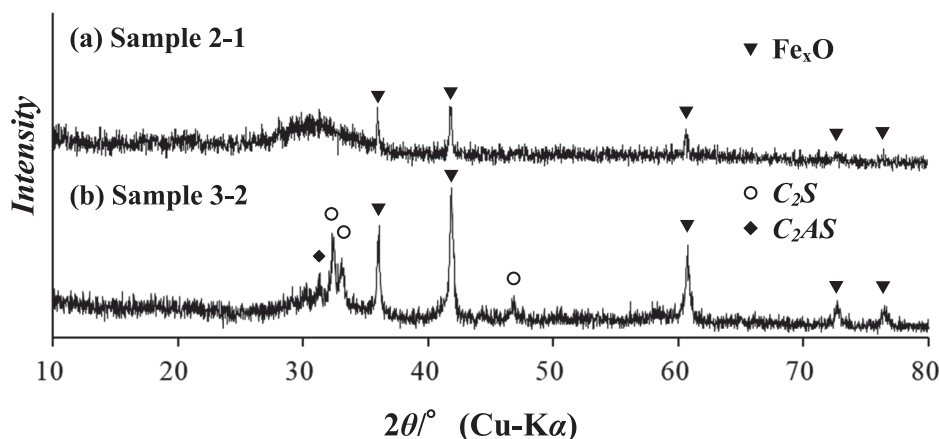


Fig. 5. X-ray diffraction patterns of slag samples.

Table 2. Experimental results at 1 673 K.

No.	n_{CaO}/n_{NS}	mass%Fe ²⁺	mass%Fe ^{total}	$X_{Fe,O}$	emf/mV	$\log(P_{O_2}/atm)$	$a_{Fe,O}$	Phase
1-1	0.117	27.5	30.0	0.380	97.05	-10.05	0.638	L
1-2		37.2	40.5	0.515	85.63	-9.91	0.749	L
1-3		38.3	42.2	0.538	85.01	-9.90	0.755	L
1-4		42.8	50.8	0.662	79.83	-9.84	0.812	L
2-1	0.520	17.7	19.6	0.240	119.50	-10.32	0.466	L
2-2		26.6	31.1	0.392	91.13	-9.98	0.693	L
2-3		33.2	36.0	0.446	86.10	-9.91	0.744	L
2-4		35.6	40.1	0.503	82.23	-9.87	0.785	L
2-5		22.8	25.9	0.321	97.43	-10.05	0.635	L
2-6		28.4	32.6	0.409	87.91	-9.94	0.725	L
2-7		33.2	37.0	0.462	84.97	-9.90	0.756	L
2-8		35.0	39.4	0.495	82.64	-9.87	0.781	L
2-9		36.7	40.9	0.512	81.05	-9.85	0.798	L
2-10		35.9	39.3	0.490	86.40	-9.92	0.741	L
2-11		35.8	40.3	0.506	85.60	-9.91	0.749	L
2-12		39.1	42.1	0.525	82.32	-9.87	0.784	L
3-1	1.05	12.6	14.0	0.167	124.84	-10.39	0.432	C ₂ S+C ₂ AS+L
3-2		17.4	18.1	0.211	112.22	-10.23	0.516	C ₂ S+C ₂ AS+L
3-3		20.5	24.3	0.299	94.82	-10.02	0.658	C ₂ S+C ₂ AS+L
3-4		20.3	21.5	0.254	100.97	-10.09	0.604	C ₂ S+C ₂ AS+L
3-5		22.1	25.3	0.308	91.63	-9.98	0.688	C ₂ S+C ₂ AS+L
3-6		23.5	28.0	0.346	90.82	-9.97	0.696	C ₂ S+C ₂ AS+L
3-7		20.7	24.6	0.303	99.10	-10.07	0.620	C ₂ S+C ₂ AS+L
3-8		22.6	27.4	0.340	94.07	-10.01	0.665	C ₂ S+C ₂ AS+L
3-9		25.9	30.4	0.376	88.61	-9.94	0.718	C ₂ S+C ₂ AS+L
3-10		34.5	43.5	0.554	89.30	-9.95	0.711	C ₂ S+L
3-11		38.3	47.7	0.610	83.30	-9.88	0.773	C ₂ S+L
3-12		39.5	51.2	0.660	81.95	-9.86	0.788	C ₂ S+L
3-13		39.9	50.0	0.641	80.90	-9.85	0.800	C ₂ S+L
3-14		43.7	54.1	0.695	79.30	-9.83	0.818	L
3-15		46.4	56.7	0.728	78.10	-9.82	0.832	L
3-16		48.7	60.3	0.779	78.56	-9.82	0.826	L
4-1	2.79	14.2	21.9	0.279	129.29	-10.44	0.406	C ₂ S+C ₃ S+L
4-2		17.5	27.7	0.357	121.66	-10.35	0.452	C ₂ S+L
4-3		24.8	34.7	0.439	103.46	-10.13	0.583	C ₂ S+L
4-4		37.1	45.8	0.572	86.27	-9.92	0.742	C ₂ S+L
4-5		29.5	40.1	0.506	100.04	-10.08	0.612	C ₂ S+L
4-6		30.9	45.1	0.581	89.72	-9.96	0.707	C ₂ S+L
4-7		32.1	43.9	0.559	100.59	-10.09	0.607	C ₂ S+L
4-8		36.2	47.6	0.603	84.36	-9.89	0.762	C ₂ S+L
4-9		36.7	47.1	0.595	88.92	-9.95	0.715	C ₂ S+L
4-10		39.6	51.1	0.650	83.06	-9.88	0.776	C ₂ S+L
4-11		39.9	51.6	0.655	79.03	-9.83	0.821	L
4-12		41.9	52.4	0.664	77.46	-9.81	0.839	L
5-1	11.5	34.0	47.7	0.603	121.32	-10.34	0.454	L
5-2		35.5	51.4	0.657	109.38	-10.20	0.537	L
5-3		33.4	47.6	0.603	121.78	-10.35	0.451	L
5-4		40.0	53.5	0.677	103.68	-10.13	0.581	L
5-5		41.2	53.5	0.675	107.83	-10.18	0.549	L
5-6		33.9	48.6	0.617	115.87	-10.28	0.490	L
5-7		48.1	60.6	0.771	85.69	-9.91	0.748	L
5-8		51.4	59.0	0.736	84.00	-9.89	0.766	L
5-9		50.7	61.2	0.775	81.47	-9.86	0.793	L
5-10		52.9	62.9	0.798	81.48	-9.86	0.793	L

When the standard state for Fe_xO is taken as pure non-stoichiometric liquid Fe_xO in equilibrium with pure solid iron, the activities of Fe_xO in slags, $a_{\text{Fe}_x\text{O}}$, can be obtained by

$$a_{\text{Fe}_x\text{O}} = (P_{\text{O}_2} / P_{\text{O}_2}^\circ)^{1/2} \dots\dots\dots (14)$$

, where $P_{\text{O}_2}^\circ$ is the equilibrium oxygen partial pressure for the mixture of pure solid Fe + pure non-stoichiometric liquid Fe_xO .

$$\log[P_{\text{O}_2}^\circ / \text{atm}] = 4.39 - 23\,500 / (T / \text{K})^{19) \dots\dots\dots (15)$$

The Fe_xO activities determined at 1 673 K are summarized together with the slag compositions in Table 2 and are

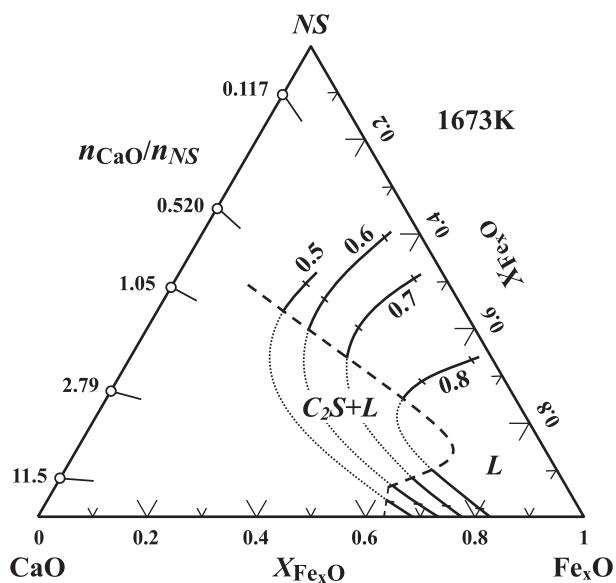


Fig. 6. Liquidus curve coexisting with Ca_2SiO_4 and iso-activity curve of Fe_xO at 1 673 K.

shown in Fig. 7.

The slags of $n_{\text{CaO}}/n_{\text{NS}} = 0.117, 0.520$ and 11.5 occur homogeneous liquids in the experimental composition ranges, and $a_{\text{Fe}_x\text{O}}$ in their slags are plotted against $X_{\text{Fe}_x\text{O}}$ in Fig. 7(a). As seen in this figure, the Fe_xO activities in the slags of $n_{\text{CaO}}/n_{\text{NS}} = 11.5$ exhibited negative deviation from Raoult's law and were very close to the reported values for CaO- Fe_xO system.^{12,20)} On the other hand, the activities in the slags of $n_{\text{CaO}}/n_{\text{NS}} = 0.117$ and 0.520 deviated positively from Raoult's law, and the smooth curves could be drawn passing through the experimental data points.

The relations between $a_{\text{Fe}_x\text{O}}$ and $X_{\text{Fe}_x\text{O}}$ for the slags of $n_{\text{CaO}}/n_{\text{NS}} = 1.05$ and 2.79 are shown in Figs. 7(b) and 7(c), respectively. For the slags of these ratios, there are the two-phase region of $\text{C}_2\text{S} + \text{L}$ and the three-phase regions of $\text{C}_2\text{S} + \text{C}_2\text{AS} + \text{L}$ or $\text{C}_2\text{S} + \text{C}_3\text{S} + \text{L}$ together with the homogeneous liquid region according to the results of the XRD studies given in Table 2. On the activity-composition curves for such heterogeneous slags, inflections would be observed at the phase boundaries,²¹⁾ although one smooth curve can be drawn in homogeneous liquid slag. Figures 7(b) and 7(c) present the activity curves which inflect at the phase boundary compositions estimated tentatively in this study.

Based on the relations between $a_{\text{Fe}_x\text{O}}$ and $X_{\text{Fe}_x\text{O}}$ in Fig. 7, the iso-activity curves in the homogeneous liquid region at 1 673 K can be illustrated on the CaO-NS- Fe_xO pseudo-ternary field, as seen in Fig. 6. As mentioned previously, it has been reported that the addition of CaF_2 increases the activities of Fe_xO .⁹⁾ The comparison of the effects of NS and CaF_2 on $a_{\text{Fe}_x\text{O}}$ is conducted in Fig. 8. This figure shows the relation between the activity coefficient of Fe_xO , $\gamma_{\text{Fe}_x\text{O}} (\equiv a_{\text{Fe}_x\text{O}} / X_{\text{Fe}_x\text{O}})$, at a fixed mole fraction of Fe_xO , i.e., $X_{\text{Fe}_x\text{O}} = 0.6$, and the ratio to substitute CaO with NS or CaF_2 . At the substitution ratios below 0.658, the replacement of CaO with NS increased the Fe_xO activity coefficient

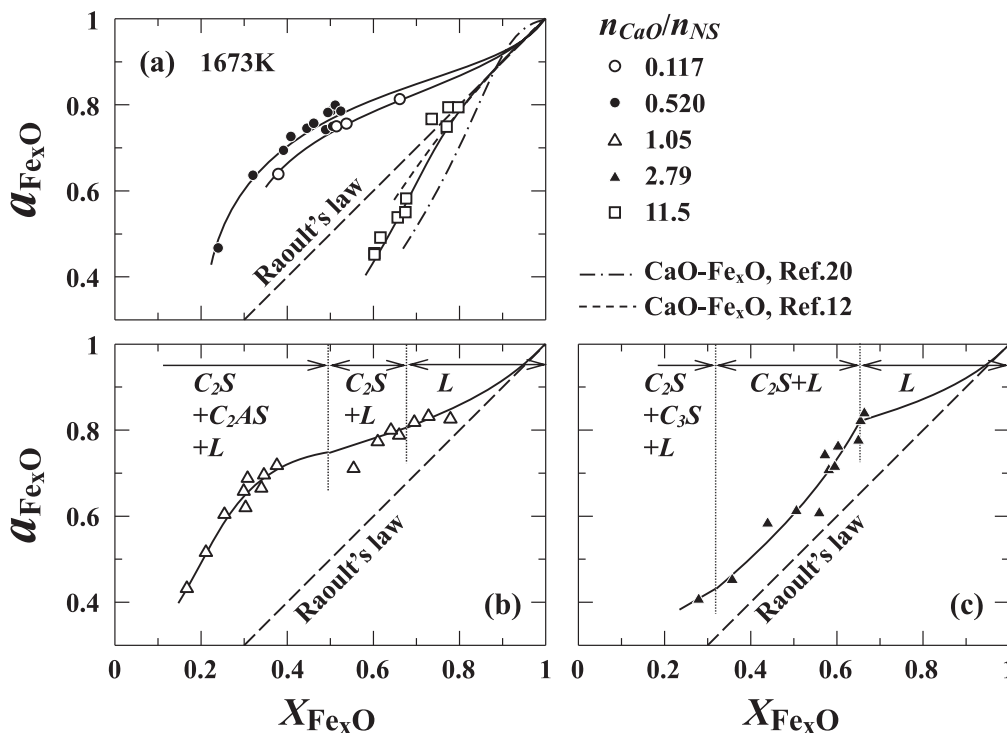


Fig. 7. Fe_xO activity plotted against Fe_xO mole fraction at 1 673 K.

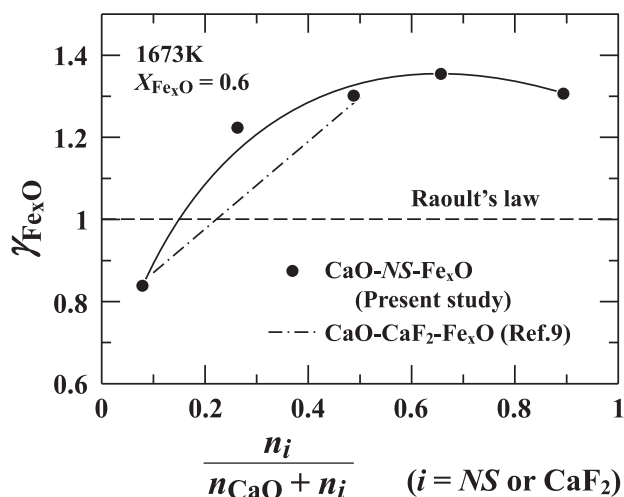
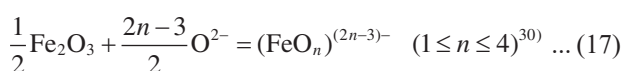


Fig. 8. Activity coefficient of Fe_xO in the CaO-nepheline syenite- Fe_xO and CaO- CaF_2 - Fe_xO pseudo-ternary systems at 1673 K.

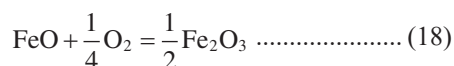
as well as CaF_2 ,⁹⁾ while $\gamma_{\text{Fe}_x\text{O}}$ decreased if the amount of NS substituted for CaO was excessive. Similar behaviors that the Fe_xO activity coefficients had maxima were reported in the other basic oxide-acidic oxide- Fe_xO systems, e.g. CaO- SiO_2 - Fe_xO ,²²⁻²⁷⁾ Na_2O - SiO_2 - Fe_xO ,²⁸⁾ and Na_2O -(SiO_2 + Al_2O_3)- Fe_xO ²⁹⁾ systems, and were often interpreted as an amphoteric property of iron oxide, as follows.²³⁾ At very acidic solutions iron oxide formed iron silicate, while at basic systems it formed ferrite; the activities were lowered in both cases, and hence there was a maximum at the intermediate region. Since NS used in this study contained 60.7 mass% SiO_2 as given in Table 1, NS would be acidic in slags. The effect of the NS addition on the slag basicity would be discussed in the next section.

3.3. $\text{Fe}^{3+}/\text{Fe}^{2+}$ Equilibrium Ratio

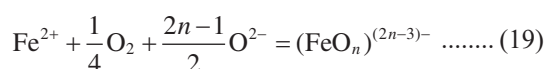
Iron oxide in slags coexisting with metallic iron has two oxidation states, i.e., FeO and Fe_2O_3 . Assuming that the complex ion of ferric iron is expressed as $(\text{FeO}_n)^{(2n-3)-}$ in silicate slags,³⁰⁾ FeO and Fe_2O_3 behave as basic and amphoteric oxides, respectively.



The chemical reaction between stoichiometric FeO and Fe_2O_3 can be given in Eq. (18).



Hence, combining Eqs. (16), (17) and (18), we obtain the following reduction-oxidation reaction.



Equation (19) implies that the ratio of $\text{Fe}^{3+}/\text{Fe}^{2+}$ increases with an increase in O^{2-} activity, i.e., slag basicity. Figure 9(a) shows the ratio of $\text{Fe}^{3+}/\text{Fe}^{2+}$ plotted against Fe_xO mole fraction in pseudo-binary systems.^{12,20,31)} In this figure, the values for optical basicity, Λ , are added next to

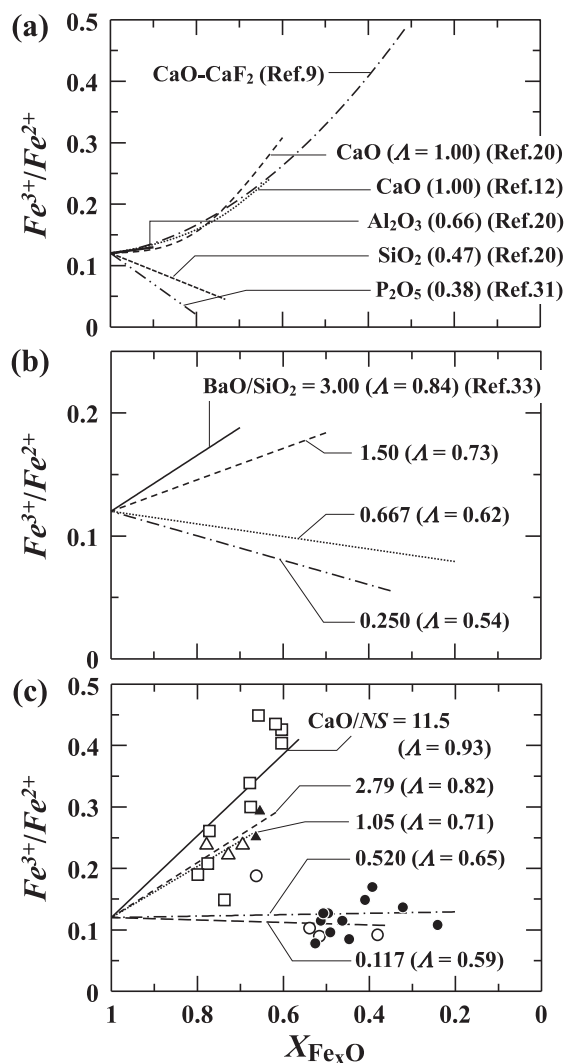


Fig. 9. Relation between $\text{Fe}^{3+}/\text{Fe}^{2+}$ ratio and $X_{\text{Fe}_x\text{O}}$ at 1673 K. (a) Fe_xO -CaO, Fe_xO - Al_2O_3 , Fe_xO - SiO_2 and Fe_xO - P_2O_5 systems, (b) BaO- SiO_2 - Fe_xO system, (c) CaO-nepheline syenite- Fe_xO system.

the chemical formulae.³²⁾ The $\text{Fe}^{3+}/\text{Fe}^{2+}$ ratio drastically increased as increasing the content of basic oxide CaO ($\Lambda = 1.00$), while the ratio decreased when acidic oxide SiO_2 ($\Lambda = 0.47$) or P_2O_5 ($\Lambda = 0.36$) was added to Fe_xO and was insensitive to the variation of the concentration of amphoteric oxide Al_2O_3 ($\Lambda = 0.66$). The $\text{Fe}^{3+}/\text{Fe}^{2+}$ ratio in the BaO- SiO_2 - Fe_xO pseudo-ternary system³³⁾ seen in Fig. 9(b) also increased with an increase in the optical basicity depending on the BaO/ SiO_2 molar ratio. As demonstrated in Fig. 9(c), the behavior of the $\text{Fe}^{3+}/\text{Fe}^{2+}$ ratio in the CaO-NS- Fe_xO pseudo-ternary system investigated in this study was in very good agreement with those reported in the pseudo-binary and ternary systems. Equation (19) indicates that the ratio of $\text{Fe}^{3+}/\text{Fe}^{2+}$ depends not only on slag basicity but also on P_{O_2} . Therefore, more detailed discussions on the relation between $\text{Fe}^{3+}/\text{Fe}^{2+}$ ratio and slag basicity along an iso-activity curve of Fe_xO would be our important future subject.

Based on the present results of the phase relations (Fig. 6), FeO activities (Fig. 8) and basicity (Fig. 9) in CaO-NS- Fe_xO slags, the amount of NS as a fluidizer added to CaO in actual processes could be suggested as follows; when the CaO/NS mole ratio is less than about 5 at 1673 K, slag

becomes homogeneous liquid with higher Fe_xO activity than $\text{CaO-Fe}_x\text{O}$ binary system, and the decrease in slag basicity is minimal.

4. Conclusion

To understand the thermochemical properties of $\text{CaO-Fe}_x\text{O}$ slags with natural recourse “nepheline syenite” added as a flux, the present study has been aimed at clarifying the phase relations and measuring the Fe_xO activities at 1 673 K. The Fe_xO activity-composition relations which inflected at the phase boundaries could be drawn passing through the experimental data points. When the ratio to substitute CaO with nepheline syenite was below 0.658, nepheline syenite had the effect to increase Fe_xO activities; this trend was very similar to the $\text{CaO-CaF}_2\text{-Fe}_x\text{O}$ system. The behavior of the $\text{Fe}^{3+}/\text{Fe}^{2+}$ ratio in the $\text{CaO-nepheline syenite Fe}_x\text{O}$ pseudo-ternary system was in good agreement with those reported in the other systems of Fe_xO with basic, amphoteric or acidic oxides. Based on the experimental results in this study, when nepheline syenite is added to $\text{CaO-Fe}_x\text{O}$ slag in the range of 17 atomic% or less at 1 673 K, slag becomes homogeneous liquid with higher Fe_xO activity than $\text{CaO-Fe}_x\text{O}$ binary system, and the decrease in slag basicity is minimal.

REFERENCES

- M. Hino and K. Ito, eds.: Thermodynamic Data for Steelmaking, Tohoku University Press, Sendai, (2010), 30.
- Y. Kashiwaya and M. Hasegawa: *ISIJ Int.*, **52** (2012), 1513. <https://doi.org/10.2355/isijinternational.52.1513>
- O. F. Tuttle and J. V. Smith: *American Journal of Science*, **256** (1958), 571.
- P. W. Kingston and W. F. Caley: *Minerals Engineering*, **2** (1989), 207. [https://doi.org/10.1016/0892-6875\(89\)90041-1](https://doi.org/10.1016/0892-6875(89)90041-1)
- T. S. Tribe, P. W. Kingston, J. B. MacDonald and W. F. Caley: *Ironmaking Steelmaking*, **21** (1994), 145.
- S. Amini, M. Brungs and O. Ostrovski: *ISIJ Int.*, **47** (2007), 32. <https://doi.org/10.2355/isijinternational.47.32>
- A. F. Yang, A. Karasev and P. G. Jönsson: *Steel Res. Int.*, **87** (2016), 599. <https://doi.org/10.1002/srin.201500154>
- F. N. H. Schrama, F. Ji, A. Hunt, E. M. Beunder, R. Woolf, A. Tuling, P. Warren, J. Sietsma, R. Boom and Y. Yang: *Ironmaking Steelmaking*, **47** (2020), 464. <https://doi.org/10.1080/03019233.2020.1747778>
- M. Iwase, E. Ichise, N. Yamada and K. Nishida: *Trans. Iron Steel Soc. AIME*, **4** (1984), 47.
- H. Ozawa, M. Hasegawa, Y. Kashiwaya and M. Iwase: *Steel Res. Int.*, **81** (2010), 25. <https://doi.org/10.1002/srin.200900099>
- J. F. Schairer: *J. Geol.*, **58** (1950), 512.
- M. Iwase, N. Yamada, K. Nishida and E. Ichise: *Trans. Iron Steel Soc. AIME*, **4** (1984), 69.
- A. Muan and E. F. Osborn: Phase Equilibria among Oxides in Steelmaking, Addison-Wesley Publishing Company, Reading, MA, (1965), 90.
- JIS M 8213: 1995, Iron ores - Method for determination of acid soluble iron (II) content.
- H. Schmalzreid: *Z. Elektrochem.*, **66** (1962), 572 (in German). <https://doi.org/10.1002/bbpc.19620660710>
- M. Iwase, E. Ichise, M. Takeuchi and T. Yamasaki: *Trans. Jpn. Inst. Met.*, **25** (1984), 43. <https://doi.org/10.2320/matertrans1960.25.43>
- M. Iwase, N. Yamada, E. Ichise and H. Akizuki: *Trans. Iron Steel Soc. AIME*, **5** (1984), 53.
- M. Iwase, M. Yasuda and T. Mori: *Electrochim. Acta*, **24** (1979), 261. [https://doi.org/10.1016/0013-4686\(79\)85043-4](https://doi.org/10.1016/0013-4686(79)85043-4)
- H. Hoshino and M. Iwase: *Metall. Mater. Trans. B*, **27** (1996), 375. <https://doi.org/10.1007/BF02914900>
- S. Ban-ya, A. Chiba and A. Hikosaka: *Tetsu-to-Hagané*, **66** (1980), 1484 (in Japanese). https://doi.org/10.2355/tetsutohagane1955.66.10_1484
- S. Seetharaman, A. McLean, R. Guthrie and S. Sridhar: Treatise on Process Metallurgy Vol. 1, Elsevier, Oxford, (2014), 551.
- C. R. Taylor and J. Chipman: *Trans. AIME*, **154** (1943), 228.
- E. T. Turkdogan and J. Pearson: *J. Iron Steel Inst.*, **173** (1953), 217.
- T. Ogura, R. Fujiwara, R. Mochizuki, Y. Kawamoto, T. Oishi and M. Iwase: *Metall. Trans. B*, **23** (1992), 459. <https://doi.org/10.1007/BF02649665>
- M. Kudo, E. Jak, P. Hayes, K. Yamaguchi and Y. Takeda: *Metall. Mater. Trans. B*, **31** (2000), 15. <https://doi.org/10.1007/s11663-000-0126-8>
- P. Fredriksson and S. Seetharaman: *Steel Res. Int.*, **75** (2004), 357. <https://doi.org/10.1002/srin.200405781>
- K. Saito, Y. Oshima and M. Hasegawa: *ISIJ Int.*, **61** (2021), 697. <https://doi.org/10.2355/isijinternational.ISIJINT-2020-349>
- S. Ban-ya, M. Hino and H. Takezoe: *Tetsu-to-Hagané*, **71** (1985), 1765 (in Japanese). https://doi.org/10.2355/tetsutohagane1955.71.15_1765
- M. Hasegawa, T. Hayashi, T. Sasaki and M. Iwase: *High Temp. Mater. Process.*, **31** (2012), 415. <https://doi.org/10.1515/htmp-2012-0076>
- K. Morinaga, Y. Suginozawa and T. Yanagase: *J. Japan Inst. Metals*, **40** (1976), 480 (in Japanese). https://doi.org/10.2320/jinstmet1952.40.5_480
- S. Ban-ya and T. Watanabe: *Tetsu-to-Hagané*, **63** (1977), 1809 (in Japanese). https://doi.org/10.2355/tetsutohagane1955.63.12_1809
- T. Nakamura, Y. Ueda and J. M. Toguri: *J. Jpn. Inst. Met.*, **50** (1986), 456 (in Japanese). https://doi.org/10.2320/jinstmet1952.50.5_456
- S. Yamashita, H. Fujiwara, E. Ichise and M. Iwase: *Iron and Steel-maker*, **19** (1992), September, 57.